

# Rare hadronic $B$ decays: probing deeper into the Standard Model

A. J. Schwartz

*Physics Department, University of Cincinnati, Cincinnati, Ohio 45221*

**Abstract.** We present recent results from the Belle experiment on rare hadronic  $B$  meson decays. The results are based on a  $78 \text{ fb}^{-1}$  data sample and consist of branching fractions,  $CP$  asymmetries, and polarization amplitudes. The decays studied include two-body pseudoscalar-pseudoscalar final states ( $B \rightarrow \pi\pi$ ,  $K\pi$ ,  $KK$ , and  $D^0 K^\pm$ ); pseudoscalar-vector final states ( $B \rightarrow \omega\pi$ ,  $\omega K$ , and  $\phi K$ ); and vector-vector final states ( $B \rightarrow \phi K^*$  and  $\rho^+ \rho^0$ ).

## INTRODUCTION

Rare hadronic  $B$  decays are useful for probing physics beyond the Standard Model. Their amplitudes usually contain internal loops, which are sensitive to mass scales that cannot be accessed directly. Here we present recent measurements of such decays by the Belle experiment at KEK. This experiment runs at the KEKB asymmetric  $e^+e^-$  collider, which has a center-of-mass (CM) energy near the  $\Upsilon(4S)$  resonance. The results are from  $78 \text{ fb}^{-1}$  of data, which corresponds to  $85 \times 10^6$   $B\bar{B}$  pairs produced.

The Belle detector consists of a three-layer silicon vertex detector, a 50-layer central drift chamber (CDC) for charged-particle tracking, an array of silica aerogel threshold Čerenkov counters (ACC), time-of-flight scintillation counters (TOF), a CsI(Tl) electromagnetic calorimeter (ECL), and a superconducting solenoid providing a 1.5 T magnetic field. An iron flux-return located outside the coil is instrumented with resistive plate chambers to identify muons and  $K_L^0$ 's. For details of the detector, see Ref. [1].

Charged tracks are identified as kaons or pions by the number of photoelectrons detected in the ACC, the specific ionization energy loss ( $dE/dx$ ) in the CDC, and, if slow enough, their time-of-flight. This information is used to calculate kaon and pion relative likelihoods  $\mathcal{L}_K$  and  $\mathcal{L}_\pi$ . Tracks are identified as pions or kaons based on the likelihood ratios  $R_{K,\pi} \equiv \mathcal{L}_{K,\pi}/(\mathcal{L}_\pi + \mathcal{L}_K)$ . The efficiency for kaons is typically 84% with a pion misidentification rate of 5%; the efficiency for pions is typically 91% with a kaon misidentification rate of 10%.

For most final states there is substantial background from  $e^+e^- \rightarrow q\bar{q}$  continuum events ( $q = u, d, s, c$ ). We distinguish this background from  $B$  decays by first combining five modified Fox-Wolfram moments into a Fisher discriminant. This is then combined with a likelihood function for  $\theta_B$ , the polar angle of the  $B$  meson flight direction, and the resulting likelihood function is used to form a likelihood ratio  $R_{q\bar{q}} \equiv \mathcal{L}_{sig}/(\mathcal{L}_{sig} + \mathcal{L}_{q\bar{q}})$ . A mode-dependent cut on  $R_{q\bar{q}}$  is made to significantly reduce background events. Typical cut values reject  $\gtrsim 90\%$  of  $q\bar{q}$  background with a signal efficiency of 40–70%.

The analyses presented here proceed in three steps: (a) selecting the final state of interest using  $R_{K,\pi}$  to identify tracks as pions or kaons; (b) using  $R_{q\bar{q}}$  to reject continuum background; and (c) selecting  $B$  decays by cutting on the variables  $m_{bc} \equiv \sqrt{E_{\text{beam}}^{*2} - p_B^{*2}}$  and  $\Delta E \equiv E_B^* - E_{\text{beam}}^*$ , where  $E_{\text{beam}}^*$  denotes the beam energy and  $p_B^*$  and  $E_B^*$  denote the reconstructed momentum and energy of the candidate  $B$  meson, all evaluated in the  $e^+e^-$  CM frame. For correctly-identified  $B$  decays,  $m_{bc} = M_B$  and  $\Delta E = 0$ . Throughout this paper, charge-conjugate modes are included unless stated otherwise. When two errors are listed for a measurement, the first one is statistical and the second one systematic.

## $B \rightarrow \pi\pi/K\pi/KK$ DECAYS

These decays proceed via  $b \rightarrow u$  tree and  $b \rightarrow d,s$  loop diagrams, and the final states include both charged and neutral kaons and pions. Neutral kaons are identified via  $K_S^0 \rightarrow \pi^+\pi^-$ , and neutral pions are identified via  $\pi^0 \rightarrow \gamma\gamma$  (where the photons produce clusters in the ECL). The  $\Delta E$  distributions after all selection cuts and a cut  $5.27 < m_{bc} < 5.29 \text{ GeV}/c^2$  are shown in Fig. 1. The event yields are obtained by fitting these distributions for signal,  $q\bar{q}$  background, and other charmless  $B$  decay background. Possible reflections due to  $K^\pm/\pi^\pm$  misidentification are included where applicable. All fit parameters other than the normalizations are fixed: most are determined from Monte Carlo (MC) simulation, while others are determined directly from the data, usually from events in a lower  $m_{bc}$  sideband. The resulting event yields are listed in Table 1. The statistical significance of signals is calculated as  $\mathcal{S} = \sqrt{2\ln(L_{\text{max}}/L_0)}$ , where  $L_0$  is the likelihood obtained assuming no signal events and  $L_{\text{max}}$  is the (maximum) likelihood obtained with  $N_s$  signal events. For cases where no significant signal is observed, we quote a 90% C.L. upper limit using a Feldman-Cousins frequentist approach [2]. The corresponding branching fractions are also listed in Table 1 and show the theoretically-expected hierarchy:  $B(B \rightarrow K\pi) > B(B \rightarrow \pi\pi) > B(B \rightarrow K\bar{K})$ .

The branching fractions can be used to constrain the magnitudes of the CKM phases  $\phi_2$  and  $\phi_3$  [3]. For such constraints, ratios of partial widths are most useful because of their reduced hadronic uncertainties. We thus use the results in Table 1 and the lifetime ratio  $\tau_{B^+}/\tau_{B^0} = 1.083 \pm 0.017$  [4] to calculate the partial width ratios listed in Table 2. The fact that  $\Gamma(\pi^+\pi^-)/2\Gamma(\pi^+\pi^0) \neq 1$  implies that the penguin contribution to  $B^0 \rightarrow \pi^+\pi^-$  is significant.

For the flavor-specific decays  $B \rightarrow K^\pm\pi^\mp$ ,  $K^\pm\pi^0$ ,  $K^0\pi^\pm$ , and  $\pi^\pm\pi^0$ , the  $\Delta E$  distributions are fitted separately for  $B$  and  $\bar{B}$  candidates to measure the  $CP$  asymmetry  $A_{CP} \equiv [N(\bar{B} \rightarrow \bar{f}) - N(B \rightarrow f)] / [N(\bar{B} \rightarrow \bar{f}) + N(B \rightarrow f)]$ , where  $B(\bar{B})$  represents  $B^0$  or  $B^+$  ( $\bar{B}^0$  or  $B^-$ ). The results are listed in Table 3; no significant  $CP$  asymmetries are observed.

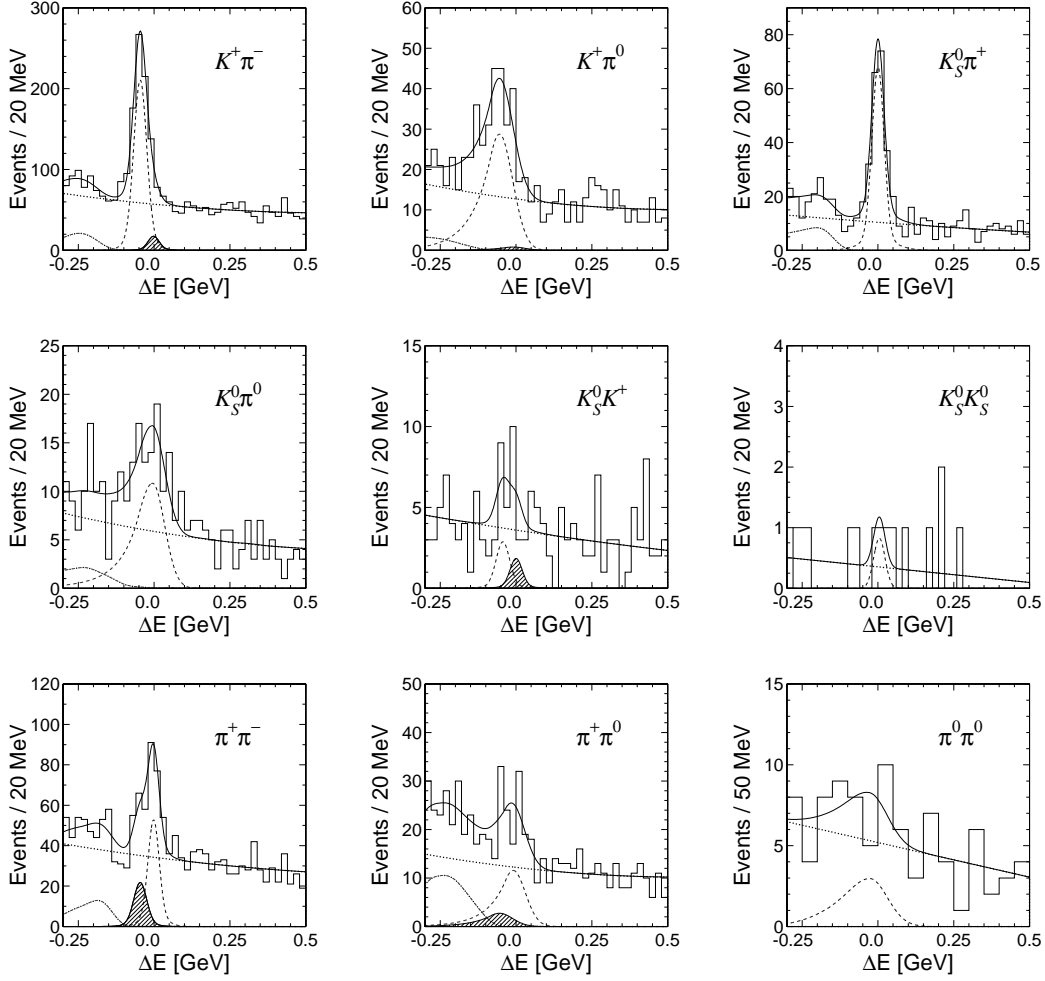


**FIGURE 1.**  $B \rightarrow hh$   $\Delta E$  distributions for  $5.27 < m_{bc} < 5.29 \text{ GeV}/c^2$ . The fit results are shown as the solid, dashed, dotted, and dash-dotted curves for the total, signal,  $q\bar{q}$  background, and  $B\bar{B}$  background, respectively. The hatched area indicates reflections resulting from  $\pi^\pm \rightarrow K^\pm$  misidentification. All tracks are assigned the pion mass; this produces the shift of signal modes containing  $K^\pm$ 's towards  $-\Delta E$  values.

## $B^\pm \rightarrow D_{CP} K^\pm$ DECAYS

The decay  $B^\pm \rightarrow D_{CP} K^\pm$ , where  $D_{CP}$  represents a  $D^0$  decaying to a  $CP$  eigenstate, proceeds via  $b \rightarrow c$  and  $b \rightarrow u$  transitions as shown in Fig. 2. Interference between the amplitudes gives rise to direct  $CP$  violation, and measuring  $A_{CP}$  allows one to constrain the CKM phase  $\phi_3$ . The observables are [6]:

$$\begin{aligned}
 A_{1,2} &\equiv \frac{B(B^- \rightarrow D_{1,2} K^-) - B(B^+ \rightarrow D_{1,2} K^+)}{B(B^- \rightarrow D_{1,2} K^-) + B(B^+ \rightarrow D_{1,2} K^+)} = \frac{2r \sin \delta' \sin \phi_3}{1 + r^2 + 2r \cos \delta' \cos \phi_3} \\
 \mathcal{R}_{1,2} &\equiv \frac{R^{D^{1,2}}}{R^{D^0}} = 1 + r^2 + 2r \cos \delta' \cos \phi_3,
 \end{aligned} \tag{1}$$

**TABLE 1.** Event yields, signal significance, efficiencies, and branching fractions (90% C.L. upper limits) for  $B \rightarrow hh$  decays.

Mode	$N_s$	$\mathcal{S}$	$\epsilon$ (%)	$B \times 10^6$ (90% C.L. limit)
$\pi^+ \pi^-$	$133^{+19}_{-18}$	8.5	35.2	$4.4 \pm 0.6 \pm 0.3$
$\pi^+ \pi^0$	$72.4 \pm 17.4$	4.5	16.1	$5.3 \pm 1.3 \pm 0.5$
$\pi^0 \pi^0$	$12.0^{+9.1}_{-8.6}$	1.9	7.8	$1.8^{+1.4+0.5}_{-1.3-0.7}$ ( $< 4.4$ )
$K^+ \pi^-$	$596 \pm 33$	24.1	37.9	$18.5 \pm 1.0 \pm 0.7$
$K^+ \pi^0$	$199 \pm 22$	10.8	18.3	$12.8 \pm 1.4^{+1.4}_{-1.0}$
$K^0 \pi^+$	$187 \pm 16$	16.4	10.0	$22.0 \pm 1.9 \pm 1.1$
$K^0 \pi^0$	$72.6 \pm 14.0$	5.8	6.8	$12.6 \pm 2.4 \pm 1.4$
$K^+ K^-$	$-1.0^{+6.6}_{-5.9}$	—	20.1	$< 0.7$
$K^+ \overline{K}^0$	$8.6 \pm 5.9$	1.6	5.9	$1.7 \pm 1.2 \pm 0.1$ ( $< 3.4$ )
$K^0 \overline{K}^0$	$2.0 \pm 1.9$	1.3	2.9	$0.8 \pm 0.8 \pm 0.1$ ( $< 3.2$ )

**TABLE 2.** Partial width ratios for  $B \rightarrow hh$ .

Ratio	Measured Value
$\Gamma(\pi^+ \pi^-)/2\Gamma(\pi^+ \pi^0)$	$0.45 \pm 0.13 \pm 0.05$
$\Gamma(\pi^+ \pi^-)/\Gamma(K^+ \pi^-)$	$0.24 \pm 0.04 \pm 0.02$
$\Gamma(\pi^0 \pi^0)/\Gamma(\pi^+ \pi^0)$	$< 0.92$ @ 90% C.L.
$2\Gamma(K^+ \pi^0)/\Gamma(K^0 \pi^+)$	$1.16 \pm 0.16^{+0.14}_{-0.11}$
$\Gamma(K^+ \pi^-)/\Gamma(K^0 \pi^+)$	$0.91 \pm 0.09 \pm 0.06$
$\Gamma(K^+ \pi^-)/2\Gamma(K^0 \pi^0)$	$0.74 \pm 0.15 \pm 0.09$

where  $\delta' = \delta(\delta + \pi)$  for  $D_1$  ( $D_2$ ) and the ratios  $R^{D^{1,2}}$  and  $R^{D^0}$  are:

$$\begin{aligned}
R^{D^{1,2}} &= \frac{B(B^- \rightarrow D_{1,2} K^-) + B(B^+ \rightarrow D_{1,2} K^+)}{B(B^- \rightarrow D_{1,2} \pi^-) + B(B^+ \rightarrow D_{1,2} \pi^+)} \\
R^{D^0} &= \frac{B(B^- \rightarrow D^0 K^-) + B(B^+ \rightarrow \overline{D}^0 K^+)}{B(B^- \rightarrow D^0 \pi^-) + B(B^+ \rightarrow \overline{D}^0 \pi^+)}.
\end{aligned}$$

**TABLE 3.** CP asymmetries for  $B \rightarrow hh$ . For  $B^0 \rightarrow \pi^+ \pi^-$ , see [5] ( $t$ -dependent analysis).

Mode	$N_s(\overline{B})$	$N_s(B)$	$A_{CP}$	90% C.L. Interval
$\pi^+ \pi^0$	$31.2 \pm 11.9$	$41.3 \pm 12.7$	$-0.14 \pm 0.24^{+0.05}_{-0.04}$	$(-0.57, 0.30)$
$K^+ \pi^-$	$235.4^{+19.8}_{-19.1}$	$270.2^{+19.7}_{-18.9}$	$-0.07 \pm 0.06 \pm 0.01$	$(-0.18, 0.04)$
$K^+ \pi^0$	$122.0 \pm 15.8$	$76.5 \pm 14.5$	$0.23 \pm 0.11^{+0.01}_{-0.04}$	$(-0.01, 0.42)$
$K^0 \pi^+$	$119.1^{+13.8}_{-13.1}$	$104.4^{+13.2}_{-12.5}$	$0.07^{+0.09+0.01}_{-0.08-0.03}$	$(-0.10, 0.22)$

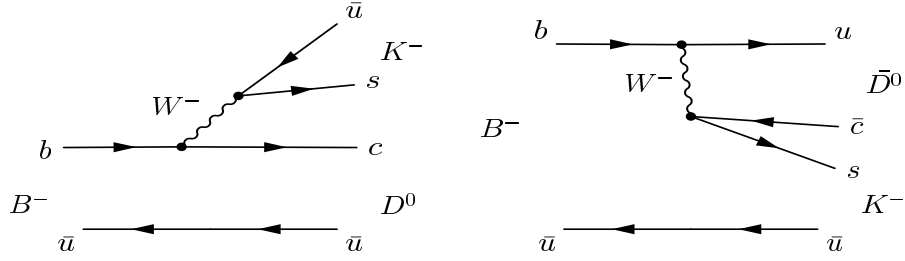


**FIGURE 2.** Feynman diagrams for  $B^\pm \rightarrow D_{CP} K^\pm$ :  $b \rightarrow c$  tree (left) and  $b \rightarrow u$  tree (right).

In these expressions,  $D_1$  and  $D_2$  are  $CP$ -even and  $CP$ -odd eigenstates, respectively, of the neutral  $D^0$  meson;  $r$  is the ratio of the  $b \rightarrow u$  and  $b \rightarrow c$  amplitudes shown in Fig. 2; and  $\delta$  is their strong phase difference. The ratio  $r$  is expected to be only  $\sim 0.1$  due to a CKM suppression factor and a color suppression factor. The ratio  $R^{D^0}$  has been previously measured by Belle ( $0.079 \pm 0.009 \pm 0.006$  [7]) and CLEO ( $0.099^{+0.014+0.007}_{-0.012-0.006}$  [8]). The results are in agreement with naive factorization:  $\tan^2 \theta_C (f_K/f_\pi)^2 \approx 0.074$ . Here we present new results for  $R^{D^0}$ ,  $R^{D^{1,2}}$ , and  $A_{1,2}$ ; these values can be inserted into Eq. (1) to determine the three unknowns  $r$ ,  $\delta$ , and  $\phi_3$ .

For this analysis  $D^0$  mesons are reconstructed as  $K^-\pi^+$ ;  $D_1$  mesons ( $CP = +1$ ) as  $K^+K^-$  and  $\pi^+\pi^-$ ; and  $D_2$  mesons ( $CP = -1$ ) as  $K_S^0\pi^0$ ,  $K_S^0\phi$ ,  $K_S^0\omega$ ,  $K_S^0\eta$ , and  $K_S^0\eta'$ . The short-lived mesons are reconstructed as follows:  $\phi \rightarrow K^+K^-$  with  $1.008 < m_{KK} < 1.032$  GeV/ $c^2$ ;  $\omega \rightarrow \pi^+\pi^-\pi^0$  with  $0.732 < m_{\pi\pi\pi} < 0.820$  GeV/ $c^2$ ;  $\eta \rightarrow \gamma\gamma$  with  $0.495 < m_{\gamma\gamma} < 0.578$  GeV/ $c^2$ ; and  $\eta' \rightarrow \eta\pi^+\pi^-$  with  $0.903 < m_{\eta\pi\pi} < 1.002$  GeV/ $c^2$ . The resulting  $D^0$  candidates are required to have masses within  $2.5\sigma$  of  $m_{D^0}$ , where  $\sigma$  is the measured mass resolution (4.5–18 MeV/ $c^2$ ). The  $D^0$  and  $\pi^+/K^+$  candidates are combined to form  $B^+$  candidates by selecting combinations with  $5.27 < m_{bc} < 5.29$  GeV/ $c^2$  and  $|\Delta E| < 0.20$  GeV. The event yields are obtained from fits to the  $\Delta E$  distributions. The results for  $R^{D^0}$ ,  $R^{D^{1,2}}$ , and  $A_{1,2}$  are listed in Table 4; all  $CP$  asymmetries are consistent with zero. The factor  $r$  can be calculated via  $\mathcal{R}_1 + \mathcal{R}_2 = 2(1 + r^2)$ ; the result is  $r^2 = 0.31 \pm 0.21$ , which is only  $1.5\sigma$  from zero. Since, in Eq. (1),  $\cos \phi_3$  and  $\sin \phi_3$  are always multiplied by a factor of  $r$ , the value of  $r$  obtained precludes setting a stringent constraint upon  $\phi_3$  with the current statistics. The situation should improve with more data.

## $B \rightarrow \omega K / \omega \pi$ DECAYS

The decays  $B \rightarrow \omega K$  and  $B \rightarrow \omega \pi$  also proceed via  $b \rightarrow u$  tree and  $b \rightarrow s$  loop diagrams. Theoretical calculations based on QCD factorization [9, 10, 11, 12] predict  $B(B \rightarrow \omega \pi) \approx 2 \times B(B \rightarrow \omega K)$ . A previous Belle measurement [13] based on  $29 \text{ fb}^{-1}$  of data did not agree with this prediction, and we update that result here.

Candidate events are selected by first selecting  $\omega \rightarrow \pi^+\pi^-\pi^0$  decays. The  $\pi^0$  is reconstructed from  $\gamma\gamma$  pairs having  $|m_{\gamma\gamma} - m_{\pi^0}| < 3\sigma$  ( $\sigma = 5.4$  MeV/ $c^2$ ); each  $\gamma$  must

**TABLE 4.** Results for  $A_{CP}$  (top) and  $R^{D^0}, R^{D^{1,2}}$  (bottom).

Mode	$A_{CP}$	90% C.L. Interval
$D^0 K^\pm$	$0.04 \pm 0.06 \pm 0.03$	$(-0.07, 0.15)$
$D_1 K^\pm$	$0.06 \pm 0.19 \pm 0.04$	$(-0.26, 0.38)$
$D_2 K^\pm$	$-0.19 \pm 0.17 \pm 0.05$	$(-0.47, 0.11)$
$R^{D^0}$	$0.077 \pm 0.005 \pm 0.006$	
$R^{D^1}$	$0.093 \pm 0.018 \pm 0.008$	
$R^{D^2}$	$0.108 \pm 0.019 \pm 0.007$	

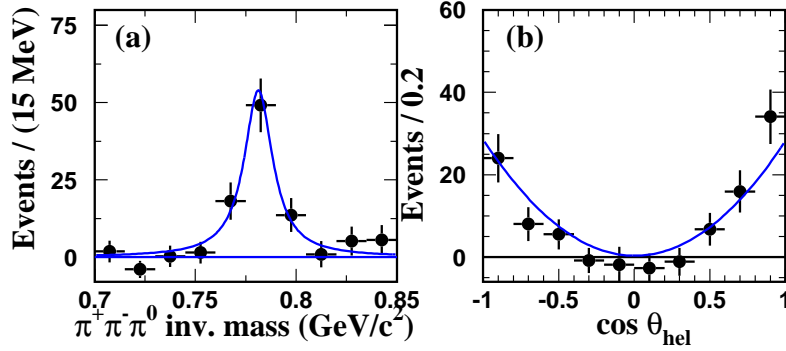


**FIGURE 3.** The fitted event yields in bins of  $m_{\pi^+\pi^-\pi^0}$  (left) and  $\cos \theta_h$  (right) for  $B \rightarrow \omega K$  and  $B \rightarrow \omega \pi$ .

also satisfy  $E_\gamma > 50$  MeV. We then require  $|m_{\pi\pi\pi} - m_\omega| < 30$  MeV/ $c^2$  ( $2\sigma$ ), and the  $\omega$  is paired with a  $\pi^\pm$ ,  $\pi^0$ ,  $K^\pm$ , or  $K_S^0$  to form  $B$  candidates. Those candidates satisfying  $5.20 < m_{bc} < 5.30$  GeV/ $c^2$  and  $|\Delta E| < 0.25$  GeV are subjected to an unbinned maximum likelihood (ML) fit using  $m_{bc}$  and  $\Delta E$  as the independent variables. The event yields resulting from the fit and the corresponding branching fractions are listed in Table 5. We note that the central value for  $B(B \rightarrow \omega K)$  is still greater than that for  $B(B \rightarrow \omega \pi)$ , in contrast with the theoretical prediction.

The main background is due to  $q\bar{q}$  continuum events. To reduce this we cut on both  $R_{q\bar{q}}$  and the helicity angle  $\theta_h$ , which is defined as the angle between the  $B$  flight direction and the vector perpendicular to the  $\omega$  decay plane, in the  $\omega$  rest frame. The cut chosen is  $|\cos \theta_h| > 0.5$ . To confirm that signal candidates contain real  $\omega$  decays, we relax the  $m_{\pi^+\pi^-\pi^0}$  cut and repeat the fits for different  $m_{\pi^+\pi^-\pi^0}$  bins. The resulting event yields are plotted in Fig. 3 and display a sharp peak at  $m_\omega$  with negligible nonresonant background underneath.

Since the  $B^\pm \rightarrow \omega h^\pm$  final states are self-tagging, we divide these samples into  $B^+$  and  $B^-$  decays and search for a  $CP$  asymmetry. The quantity measured is  $A_{CP} = [N(B^-) - N(B^+)] / [N(B^-) + N(B^+)]$ . The event yields are determined from a two-dimensional binned fit in the  $m_{bc}$ - $\Delta E$  plane. The results are listed in Table 6. While

**TABLE 5.**  $B \rightarrow \omega K$  and  $B \rightarrow \omega \pi$  event yields, statistical significance, and branching fractions (90% C.L. limits).

Mode	$N_s$	$\mathcal{S}$	$B \times 10^6$ (90% C.L. limit)
$\omega K^-$	$46.1^{+9.1}_{-8.4}$	7.8	$6.7^{+1.3}_{-1.2} \pm 0.6$
$\omega K^0$	$11.1^{+5.2}_{-4.4}$	3.2	$4.0^{+1.9}_{-1.6} \pm 0.5$ ( $< 7.6$ )
$\omega \pi^-$	$42.1^{+10.1}_{-9.3}$	6.0	$5.7^{+1.4}_{-1.3} \pm 0.6$
$\omega \pi^0$	$0.0^{+2.1}_{-0.0}$	—	( $< 1.9$ )

**TABLE 6.**  $B^\pm \rightarrow \omega K^\pm$  and  $B^\pm \rightarrow \omega \pi^\pm$  event yields separated by charge, and the resulting  $CP$  asymmetry.

Mode	$N(B^-)$	$N(B^+)$	$A_{CP}$	90% C.L. Interval
$\omega K^\pm$	$24.3^{+6.7}_{-5.9}$	$21.8^{+6.4}_{-5.7}$	$0.06^{+0.20}_{-0.18} \pm 0.01$	$(-0.25, 0.40)$
$\omega \pi^\pm$	$32.5^{+8.2}_{-7.5}$	$11.5^{+6.1}_{-5.3}$	$0.48^{+0.23}_{-0.20} \pm 0.02$	$(0.14, 0.86)$

$A_{CP}(\omega K)$  is consistent with zero,  $A_{CP}(\omega \pi)$  is  $2.4\sigma$  above zero, and a symmetric 90% C.L. interval excludes  $A_{CP} = 0$ .

## $B \rightarrow \phi K / \phi K^*$ DECAYS AND POLARIZATION

The decays  $B \rightarrow \phi K$  and  $B \rightarrow \phi K^*$  proceed only via loop diagrams ( $b \rightarrow ss\bar{s}$ ) and thus are especially sensitive to new physics. Because both the  $\phi$  and  $K^*$  are spin-1,  $B \rightarrow \phi K^*$  is a mixture of  $CP$ -even and  $CP$ -odd states; the individual components can be determined by measuring the  $\phi$  polarization.

As a first step,  $\phi \rightarrow K^+ K^-$  decays are identified by requiring pairs of oppositely-charged tracks having  $R_K > 0.1$  and  $|m_{KK} - m_\phi| < 10 \text{ MeV}/c^2$ .  $K^*$  decays are reconstructed via  $K^{*+} \rightarrow K^+ \pi^0$ ,  $K^{*+} \rightarrow K_S^0 \pi^+$ , and  $K^{*0} \rightarrow K^+ \pi^-$ ; the resulting two-body mass is required to be within  $70 \text{ MeV}/c^2$  of  $m_{K^*}$ .  $B \rightarrow \phi K$  ( $B \rightarrow \phi K^*$ ) decays are selected by pairing a  $\phi$  candidate with a  $K$  ( $K^*$ ) candidate and requiring that they be within the signal region  $5.271 < m_{bc} < 5.289$  ( $5.270 - 5.290$ )  $\text{GeV}/c^2$  and  $|\Delta E| < 0.64$  ( $0.60$ )  $\text{GeV}$ . The  $\Delta E$  window is slightly larger for  $K^{*+} \rightarrow K^+ \pi^0$  decays due to shower leakage.

The dominant background is due to  $q\bar{q}$  continuum events. There is also 5–9% contamination of  $B \rightarrow \phi K^{(*)}$  decays from nonresonant  $B \rightarrow K^+ K^- K^{(*)}$ , and 2–12% contamination from  $B \rightarrow f(980) K^{(*)}$ ,  $f(980) \rightarrow K^+ K^-$ . The uncertainty in the intrinsic width of the  $f_0(980)$  is included in the systematic error.

The signal yields are obtained via an unbinned ML fit with  $m_{bc}$  and  $\Delta E$  as the independent variables. The results and corresponding branching fractions are listed in Table 7. The projections of the fits are shown in Fig. 4. For the  $B \rightarrow \phi K^*$  modes, there is an additional systematic error due to uncertainty in the  $K^*$  polarization and the

**TABLE 7.** Branching fractions and  $CP$  asymmetries for  $B \rightarrow \phi K$  and  $B \rightarrow \phi K^*$  decays.

Mode	$N_s$	$B \times 10^6$	$A_{CP}$	90% C.L. Interval
$\phi K^+$	$136^{+16}_{-15}$	$9.4 \pm 1.1 \pm 0.7$	$0.01 \pm 0.12 \pm 0.05$	$(-0.20, 0.22)$
$\phi K^0$	$35.6^{+8.4}_{-7.4}$	$9.0^{+2.2}_{-1.8} \pm 0.7$	—	—
$\phi K^{*0}$	$58.5^{+9.1}_{-8.1}$	$10.0^{+1.6+0.7}_{-1.5-1.8}$	$0.07 \pm 0.15^{+0.05}_{-0.03}$	$(-0.18, 0.33)$
$\phi K^{*+}$	$\left\{ \begin{array}{l} 8.0^{+4.3}_{-3.5} \quad (K^+ \pi^0) \\ 11.3^{+4.5}_{-3.8} \quad (K_S^0 \pi^+) \end{array} \right.$	$6.7^{+2.1+0.7}_{-1.9-1.0}$	$-0.13 \pm 0.29^{+0.08}_{-0.11}$	$(-0.64, 0.36)$

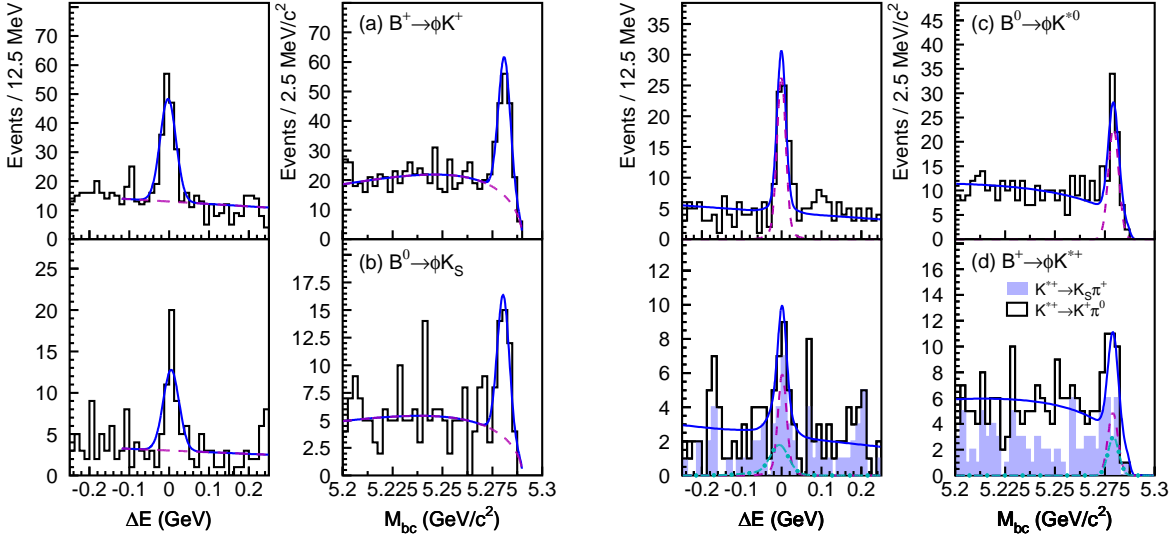


**FIGURE 4.** Projections of the unbinned ML fits for  $B \rightarrow \phi K$  decays (left) and  $B \rightarrow \phi K^*$  decays (right). The histograms show the data. Events in the  $m_{bc}$  plots are required to have  $|\Delta E|$  within the signal region, and events in the  $\Delta E$  plots are required to have  $m_{bc}$  within the signal region (see text).

corresponding uncertainty in the daughter  $\pi$  detection efficiency.

For the self-tagging modes  $B^\pm \rightarrow \phi K^{(*)\pm}$  we measure  $A_{CP} = [N(\bar{B}) - N(B)] / [N(\bar{B}) + N(B)]$ , where  $B(\bar{B})$  is  $B^0$  or  $B^+$  ( $\bar{B}^0$  or  $B^-$ ). The results are also listed in Table 7 and in all cases are consistent with zero.

The polarization of the  $\phi$  in  $B \rightarrow \phi K^*$  decays is measured using the transversity basis [14]. In this basis the  $\phi$  is at rest. The  $x$ - $y$  plane is defined by the  $K^{*0}$  daughters, with the  $-x$  axis along the direction of the  $K^*$  (see Fig. 5). The angle  $\theta_{K^*}$  is that between the  $K^{*0}$  direction and the  $K^+$  daughter. The angles  $\theta_{tr}$  and  $\phi_{tr}$  are the polar and azimuthal angles, respectively, of the  $K^+$  daughter of the  $\phi$ . The decay distribution is given by [15]:

$$\frac{d^3\Gamma(\phi_{tr}, \cos\theta_{tr}, \cos\theta_{K^*})}{d\phi_{tr}d\cos\theta_{tr}d\cos\theta_{K^*}} = \frac{9}{32\pi} \left[ |A_\perp|^2 2\cos^2\theta_{tr}\sin^2\theta_{K^*} \right. \\ \left. + |A_\parallel|^2 2\sin^2\theta_{tr}\sin^2\phi_{tr}\sin^2\theta_{K^*} \right]$$

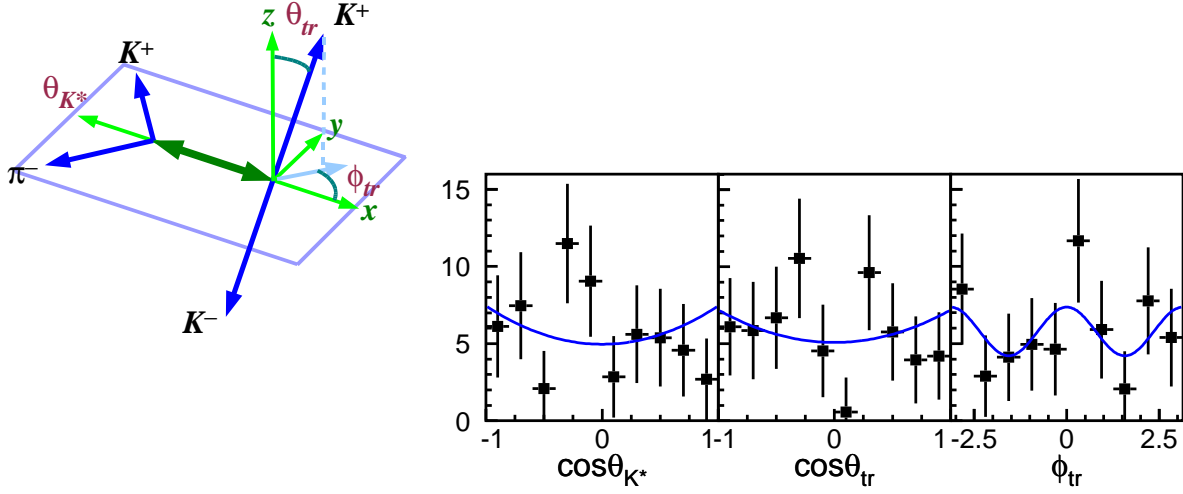


**FIGURE 5.** Definition of the angles  $\theta_{K^*}$ ,  $\theta_{tr}$ , and  $\phi_{tr}$  in the transversity basis (left), and projections of the unbinned fit for these angles (right).

$$\begin{aligned}
& + |A_0|^2 4 \sin^2 \theta_{tr} \cos^2 \phi_{tr} \cos^2 \theta_{K^*} \\
& + \sqrt{2} \text{Re}(A_{\parallel}^* A_0) \sin^2 \theta_{tr} \sin 2\phi_{tr} \sin 2\theta_{K^*} \\
& - \eta \sqrt{2} \text{Im}(A_0^* A_{\perp}) \sin 2\theta_{tr} \cos \phi_{tr} \sin 2\theta_{K^*} \\
& - 2\eta \text{Im}(A_{\parallel}^* A_{\perp}) \sin 2\theta_{tr} \sin \phi_{tr} \sin^2 \theta_{K^*} \Big], \quad (2)
\end{aligned}$$

where  $A_0$ ,  $A_{\parallel}$ , and  $A_{\perp}$  are the complex amplitudes of the three helicity states, and  $\eta = +1$  ( $-1$ ) for  $B^0$  ( $\bar{B}^0$ ) decays. The amplitude  $A_0$  denotes the longitudinal polarization of the final state, and  $A_{\perp}$  ( $A_{\parallel}$ ) denotes the transverse polarization along the  $z$  ( $y$ ) axis. Note that  $|A_0|^2 + |A_{\parallel}|^2 + |A_{\perp}|^2 = 1$ . The value of  $|A_{\perp}|^2$  ( $1 - |A_{\perp}|^2 = |A_0|^2 + |A_{\parallel}|^2$ ) is the  $CP$ -odd ( $CP$ -even) fraction of the decay.

The complex amplitudes  $A_0$ ,  $A_{\perp}$ , and  $A_{\parallel}$  are determined via an unbinned ML fit to the candidates within the  $m_{bc}$ - $\Delta E$  signal region; the probability density function for signal is given by Eq. (2). By convention, the value of  $\text{Arg}(A_0)$  is set to zero and  $|A_{\parallel}|^2$  is calculated from the normalization constraint. The results of the fit are:  $|A_0|^2 = 0.43 \pm 0.09 \pm 0.04$ ,  $|A_{\perp}|^2 = 0.41 \pm 0.10 \pm 0.04$ ,  $\text{Arg}(A_{\parallel}) = -2.57 \pm 0.39 \pm 0.09$ , and  $\text{Arg}(A_{\perp}) = 0.48 \pm 0.32 \pm 0.06$ . The projections of the fit are shown in Fig. 5. The systematic errors include the (slow) pion detection efficiency (3–6%) and background from higher  $K^*$  states (6–9%). The value of  $|A_{\perp}|^2$  obtained indicates that both  $CP$ -odd and  $CP$ -even components of  $B \rightarrow \phi K^*$  are sizable.

## $B^\pm \rightarrow \rho^\pm \rho^0$ DECAYS

The decay  $B^+ \rightarrow \rho^+ \rho^0$  proceeds via  $b \rightarrow d$  loop and  $b \rightarrow u$  tree diagrams and contains two vector mesons in the final state. Angular correlations among the decay products ( $\pi^+ \pi^0 \pi^+ \pi^-$ ) can be used to search for  $CP$ - and  $T$ -violating effects. In the final state, both  $\rho$ 's are either longitudinally or transversely polarized; the corresponding amplitudes are denoted  $H_{00}$  and  $H_{11}$ , respectively.

In this analysis,  $\rho^+ \rho^0$  states are reconstructed by combining three charged pions with one neutral pion. The charged pions are required to have  $p_T > 0.10$  GeV/ $c$ . Candidate  $\pi^0$ 's are reconstructed from  $\gamma\gamma$  pairs having  $118 < m_{\gamma\gamma} < 150$  MeV/ $c^2$ ; each  $\gamma$  must also satisfy  $E_\gamma > 50$  (100) MeV in the barrel (endcap) region. Candidate  $\rho$  mesons are identified via  $\pi^+ \pi^-$  or  $\pi^+ \pi^0$  pairs having  $0.65 < m_{\pi\pi} < 0.89$  GeV/ $c^2$ .  $B^+ \rightarrow \rho^+ \rho^0$  candidates are identified by requiring  $5.272 < m_{bc} < 5.290$  GeV/ $c^2$  and  $-0.10 < \Delta E < 0.06$  GeV. The  $H_{00}$  amplitude gives rise to asymmetric  $\rho \rightarrow \pi\pi$  decays, i.e., one pion has high momentum and the other has low momentum. The  $H_{11}$  amplitude gives rise to symmetric  $\rho \rightarrow \pi\pi$  decays. Thus, the  $H_{00}$  state has a lower reconstruction efficiency and a  $\Delta E$  resolution  $\sim 15\%$  broader than that for  $H_{11}$ .

There are large backgrounds due to  $q\bar{q}$  continuum events. To reduce these we cut on both  $R_{q\bar{q}}$  and the thrust angle  $\theta_{thr}$ , which is the angle between the thrust axis of tracks originating from the  $B$  candidate and that of the remaining tracks in the event. The cut chosen is  $|\cos \theta_{thr}| < 0.80$ . The overall rejection of continuum events is  $> 99.5\%$ , with a signal efficiency of 28%. There is also a small level of background from  $b \rightarrow c$  processes and rarer  $B$  decays such as  $B^+ \rightarrow \eta' \rho^+, K^{*+} \rho^0, \rho^+ K^{*0}$  and  $\rho\pi$ ; these tend to be displaced in  $\Delta E$ .

The resulting  $\Delta E$  and  $m_{bc}$  distributions are shown in Fig. 6. The event yields are determined by fitting in  $\Delta E$ . The fit yields  $58.7 \pm 13.2$  events with a statistical significance ( $\sqrt{2 \ln [L_{max}/L_0]}$ ) of 5.3. Fitting the  $\Delta E$  distributions for different  $m_{\pi\pi}$  bins gives the event yields plotted in Fig. 7. These distributions agree well with MC expectations and show little nonresonant background beneath the  $\rho$  peaks.

The relative strengths of  $H_{00}$  and  $H_{11}$  are determined by studying distributions of the helicity angle  $\theta_{hel}$ , which is the angle between the  $\rho$  flight direction in the  $B$  rest frame and the  $\pi^+$  flight direction in the  $\rho$  rest frame. The signal yields determined from  $\Delta E$  fits for different  $\cos \theta_{hel}$  bins are plotted in Fig. 8 for both the  $\rho^0$  and  $\rho^+$ . We perform simultaneous binned fits to these distributions using MC expectations for the  $H_{00}$  and  $H_{11}$  helicity states. The fit yields the fraction of  $\rho^0 \rho^+$  final states that are longitudinally polarized:

$$\frac{\Gamma_L}{\Gamma_{tot}} = (94.8 \pm 10.6 \pm 2.1) \%.$$

This result shows that the  $H_{00}$  state dominates, which is consistent with theoretical expectations [16]. The systematic error includes uncertainties in signal yield extraction and the polarization dependence of the detection efficiency. Based on this polarization ratio and the MC-determined reconstruction efficiencies of the two helicity states, we calculate  $B(B^+ \rightarrow \rho^+ \rho^0) = (3.17 \pm 0.71_{-0.67}^{+0.38}) \times 10^{-5}$ .

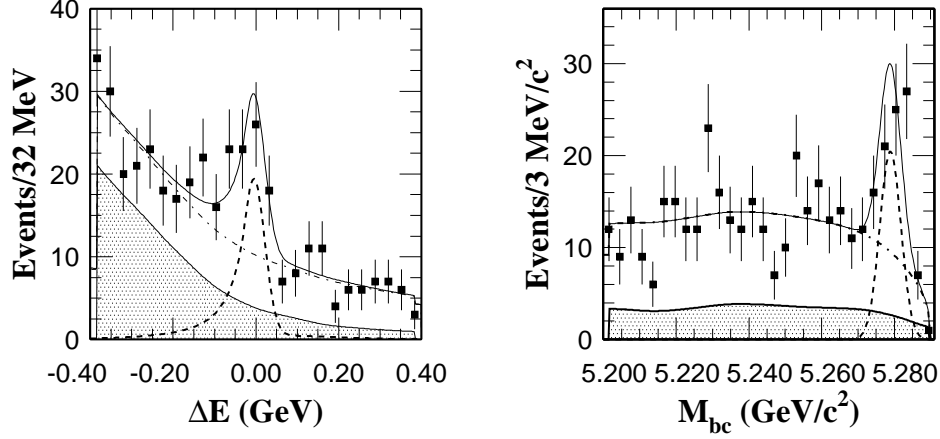


**FIGURE 6.**  $\Delta E$  (left) and  $m_{bc}$  (right) fits for candidate  $B^+ \rightarrow \rho^+ \rho^0$  decays. The shaded curve represents  $B\bar{B}$  background, the dash-dotted curve represents the sum of  $B\bar{B}$  and continuum backgrounds, the dashed curve represents the  $B^+ \rightarrow \rho^+ \rho^0$  signal, and the solid curve represents the overall sum.

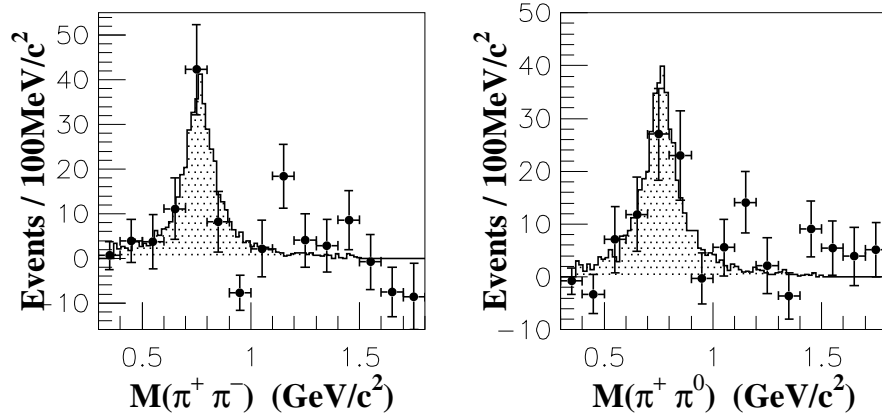


**FIGURE 7.**  $m_{\pi^+ \pi^-}$  (left) and  $m_{\pi^+ \pi^0}$  (right) distributions for candidate  $B^+ \rightarrow \rho^+ \rho^0$  decays. The shaded histogram shows MC signal.

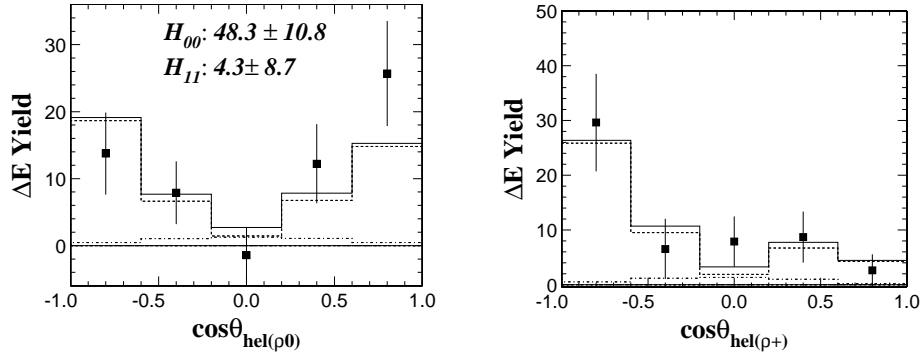


**FIGURE 8.** Helicity distributions for the  $\rho^0$  (left) and  $\rho^+$  (right) in  $B^+ \rightarrow \rho^+ \rho^0$  decays. The dashed (dash-dotted) histogram shows the  $H_{00}$  ( $H_{11}$ ) component of the fit; the solid histogram is their sum. The bin size is 0.4. The low event yield near  $\cos \theta_{hel(\rho^+)} = 1$  is due to a requirement  $p_{\pi^0}(\text{CM}) > 0.5 \text{ GeV}/c$ .

We separate the candidate events into  $B^- \rightarrow \rho^- \rho^0$  and  $B^+ \rightarrow \rho^+ \rho^0$  subsamples and fit these subsamples individually. The resulting event yields are  $29.3 \pm 9.5$  and  $29.3 \pm 9.1$ , respectively. The  $CP$  asymmetry is  $A_{CP} = [N(\rho^- \rho^0) - N(\rho^+ \rho^0)]/[N(\rho^- \rho^0) + N(\rho^+ \rho^0)] = 0.00 \pm 0.22 \pm 0.03$ , which is consistent with zero.

## SUMMARY

With  $78 \text{ fb}^{-1}$  of data the Belle experiment has:

- updated the branching fractions and  $CP$  asymmetries for  $B^0 \rightarrow \pi\pi$ ,  $B^0 \rightarrow K\pi$ , and  $B^0 \rightarrow KK$  decays;
- measured the  $CP$  asymmetries in  $B^\pm \rightarrow D_{CP} K^\pm$  decays, where  $D_{CP}$  represents a  $D^0$  decaying to a  $CP = +1$  or  $CP = -1$  eigenstate, and investigated the possibility of using the measured asymmetries to constrain the CKM phase  $\phi_3$ ;
- updated the branching fractions and  $CP$  asymmetries for  $B^\pm \rightarrow \omega\pi^\pm$  and  $B^\pm \rightarrow \omega K^\pm$  decays;
- measured the branching fractions for  $B \rightarrow \phi K$  and  $B \rightarrow \phi K^*$  decays and, for the latter, measured the polarization amplitudes  $A_\perp$ ,  $A_\parallel$ , and  $A_0$  in the transversity basis;
- measured the branching fraction for  $B^+ \rightarrow \rho^+ \rho^0$  and the helicity amplitudes  $H_{00}$  and  $H_{11}$ . This is the first reported observation of this decay.

Most results are consistent with theoretical expectations, although some channels show interesting and possibly important discrepancies at the  $2\sigma$  level. We look forward to investigating these further (and refining all of these measurements) with more data.

## REFERENCES

1. Abashian et al. (Belle Collaboration), A., *Nucl. Instr. Meth. A*, **479**, 117 (2002).
2. Feldman, G. J., and Cousins, R. D., *Phys. Rev. D*, **57**, 3873 (1998).
3. Abbaneo et al., D., “The CKM Matrix and The Unitarity Triangle,” in *Proceedings of the First Workshop on the CKM Unitarity Triangle, 13-16 Feb. 2002*, edited by M. Battaglia, A. J. Buras, P. Gambino, and A. Stocchi, CERN, hep-ph/0304132 (2003), pp. 291–308.
4. Hagiwara et al. (PDG), K., *Phys. Rev. D*, **66**, 010001 (2002).
5. Abe et al. (Belle Collaboration), K., *Phys. Rev. D*, **68**, 012001 (2003).
6. Quinn, H., and Sanda, A. I., *Eur. Phys. J.*, **C15**, 626 (2000).
7. Abe et al. (Belle Collaboration), K., *Phys. Rev. Lett.*, **87**, 111801 (2001).
8. Bornheim et al. (CLEO Collaboration), A., Tech. Rep. CLNS 03/1816, hep-ex/0302026 (2003).
9. Ali, A., Kramer, G., and Lu, C. D., *Phys. Rev. D*, **58**, 094009 (1998).
10. Chen, Y. H., Cheng, H. Y., Tseng, B., and Yang, K. C., *Phys. Rev. D*, **60**, 094014 (1999).
11. Du, D. S., Gong, H. J., Sun, J. F., and Zhu, G. H., *Phys. Rev. D*, **65**, 094025 (2002).
12. Lu, C. D., and Yang, M. Z., *Eur. Phys. J.*, **C23**, 275 (2002).
13. Lu et al. (Belle Collaboration), R. S., *Phys. Rev. Lett.*, **89**, 191801 (2002).
14. Duniety et al., I., *Phys. Rev. D*, **43**, 2193 (1991).
15. Abe, K., Satpathy, M., and Yamamoto, H., Tech. Rep. UH-511-982-01, hep-ex/0103002 (2001).
16. Aleksan et al., R., *Phys. Lett. B*, **356**, 95 (1995).